Renewable Energy 215 (2023) 118913

Contents lists available at ScienceDirect

Renewable Energy

journal homepage: www.elsevier.com/locate/renene

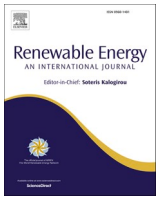

Performance degradation decomposition-ensemble prediction of PEMFC using CEEMDAN and dual data-driven model

Changzhi Li [a], Wei Lin [a], Hangyu Wu [b], Yang Li [a], Wenchao Zhu [a,b,d,*], Changjun Xie [a,b,c,*], Hoay Beng Gooi [d], Bo Zhao [e], Leiqi Zhang [e]

[a] School of Automation, Wuhan University of Technology, Wuhan, 430070, China
[b] Hubei Key Laboratory of Advanced Technology for Automotive Components, Wuhan University of Technology, Wuhan, 430070, China
[c] Modern Industry College of Artificial Intelligence and New Energy Vehicles, Wuhan University of Technology, Wuhan, 430070, China
[d] School of Electrical and Electronic Engineering, Nanyang Technological University, Singapore, 639798, Singapore
[e] State Grid Zhejiang Electric Power Research Institute, Hangzhou, 310014, China

ARTICLE INFO

Keywords:
Fuel cell
Degradation prediction
Decomposition
Hybrid framework
Attention mechanism

ABSTRACT

Proton exchange membrane fuel cells (PEMFCs) are essential modern sustainable energy generation devices. Since such an electrochemical system has a limited lifetime, accurately estimating its performance degradation is critical for practical applications. When a large amount of measurement data is available, many nonlinear forecasting methods can be used to predict the performance degradation of a PEMFC system, and the prediction accuracy can be improved by optimizing the structure and parameters of the algorithm. However, the voltage recovery phenomenon would pose a challenge to the classical data-driven methods. In this work, we propose a novel hybrid data-driven PEMFC performance prediction framework by exploring the extensive degradation information buried in the voltage decay data. With complete ensemble empirical mode decomposition with adaptive noise (CEEMDAN), the raw voltage data are first decomposed into sequences of multiple time scales. Then, the linear and nonlinear components in the decomposed sequences are predicted by autoregressive integrated moving average (ARIMA) and the attention-based gated recurrent unit (GRU), respectively. Comparative studies show that the proposed method can improve the prediction performance by 42.6%–84.2% on FC1 and 35.0%–90.6% on FC2, compared to state-of-the-art algorithms on the basis of an open-source dataset of PEMFCs.

1. Introduction

1.1. Background and literature review

Hydrogen-based proton exchange membrane fuel cells (PEMFCs) play a key role in modern sustainable and carbon-free energy systems [1–4]. The PEMFC is a clean power generation device that is environmentally friendly, lightweight, and has high power density. Therefore, it has been used in some areas, such as the military and transportation. However, the aging phenomenon and lifespan of PEMFC limit its further commercialization and large-scale applications [5–7].

Existing PEMFC prediction methods are mainly divided into data-driven and model-based methods [5]. Based on sufficient life data, the data-driven method could predict the aging process and the remaining lifetime of PEMFC, which belongs to the black box model, without considering the aging principle. Mainstream data-driven methods are mainly based on neural networks. Javed et al. [8] proposed the method of summation wavelet-extreme learning machine, which was verified on the data of the whole process from start to failure of the PEMFC stack with a useful life of 1750 h. A recurrent neural network (RNN) method was proposed by Liu et al. [9]. It used regular interval sampling and locally weighted scatterplot smoothing to realize data reconstruction and data smoothing. Using Long short-term memory (LSTM) improved the prediction accuracy by 28.46% compared to the backpropagation neural network (BPNN). Long et al. [10] used similar processing steps proposed in Ref. [9] to demonstrate that the gated recurrent unit (GRU) outperforms LSTM. Hua et al. [11] used an improved method of RNN named echo state network (ESN) for prediction. Specifically, the hidden layer in ESN was replaced by a randomly generated library reflecting the dynamic topology of neurons to improve the prediction effect. In addition to neural networks, data-driven methods include other methods as well. Wu et al. proposed a PEMFC remaining life prediction model based

* Corresponding authors. School of Automation, Wuhan University of Technology, Wuhan, 430070, China.
E-mail addresses: zhuwenchao@whut.edu.cn (W. Zhu), jackxie@whut.edu.cn (C. Xie).

https://doi.org/10.1016/j.renene.2023.118913
Received 25 February 2023; Received in revised form 5 June 2023; Accepted 11 June 2023
Available online 12 June 2023

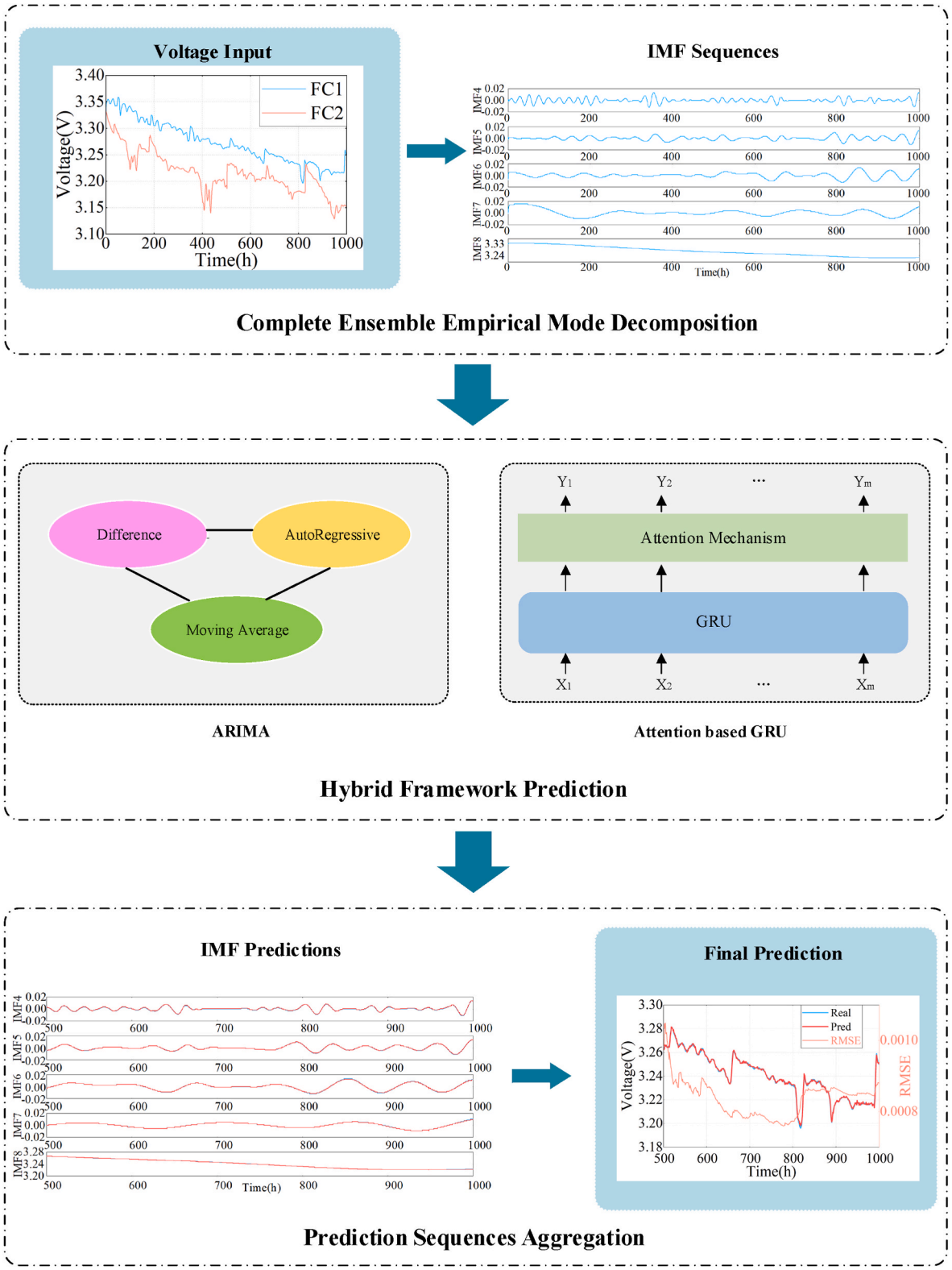

Fig. 1. Framework of the proposed hybrid framework for PEMFC performance prediction.

on a regression vector machine, where the advantages over the classical support vector machine in a small training set were shown. Ibrahim et al. [12] proposed a univariate prediction method on the basis of the discrete wavelet transform. Four methods were used to fit data features and for data reconstruction, achieving the prediction. Wang et al. [13] proposed a stacked LSTM model with two dropout parameters. They used a unique optimization algorithm to obtain the optimal model parameters which achieve the fitting of the PEMFC system degradation.

However, the data-driven method lacks consideration for the diverse aging factors of PEMFC, so the researchers also pay attention to many model-based approaches that can better reflect the physical and chemical processes involved [14,15]. For example, based on the principle of

electrochemical reaction, Zhou et al. [16] established a multi-physics aging model to predict the performance degradation of PEMFCs by considering the losses due to ohmic effects, reaction activity, and reactants mass transfer. Jahromi et al. [17] and Futter et al. [18] considered the aging of PEMFC from the component level and explained the aging principle of the catalyst layer and proton exchange membrane. A method based on pattern recognition was proposed by Liu et al. [19], which used an empirical model to extract static features from polarization curves, and then extracted the dynamic features from electrochemical impedance spectroscopy using expert knowledge and parametric modeling. Usually, only the most relevant features were selected from the entire extracted feature set.

In the model-based methods, most parameters are assumed to be constant to simplify the modeling process. However, since many aging mechanisms have not been well studied and the aging models are usually not proven, the model accuracy is usually not guaranteed under various operating conditions [19]. PEMFC has complex working mechanisms, and factors such as internal electrochemical reactions and external operating conditions would cause highly varying aging behaviors. Ma et al. [20] showed that the internal electrochemical reactions would change the temperature, gas flow, and solution conditions inside the fuel cell, leading to aging in electrodes, gas diffusion layers, catalyst layers, and proton exchange membranes. In addition, factors such as the movement and operating temperature would also affect the mechanical structure of the fuel cell, resulting in a decrease in output performance. However, due to material and design differences, the above factors have different influences on the aging process of each component. Moreover, aging time scales vary significantly between different fuel cell components, necessitating multi-time-scale modeling. For example, for rapidly aging components, the prediction model should be able to sufficiently adapt to reflect its rapid change trend while it is not needed for the slow aging process.

It should be noted that the voltage recovery phenomena in PEMFC are often ignored in model-based approaches. However, Chu et al. [21] performed a 2500h durability test on each of the three fuel cell stacks, showing that the aging of some components that lead to fuel cell performance degradation is reversible. Changes in the operating conditions may lead to a significant performance recovery in the components and the entire PEMFC system [22–25]. Considering the system output voltage, the overall performance of PEMFC shows a downward trend over time, but it would show a local mutation due to component performance recovery.

1.2. Research gap and contributions

The existing data-driven methods of PEMFC performance prediction lack the consideration of the aging mechanisms. On the other hand, since the working mechanisms of PEMFC are complicated, a physics model is usually challenging to be established and used in practical applications [20,26]. Furthermore, neither of these two categories of methods considers aging time scales with voltage recovery phenomena. Indeed, the results in recent works such as [27–29] show that the prediction accuracy of data-driven methods could be further improved by combining with the changing trend of the data with linear and nonlinear characteristics. The voltage of PEMFC shows an overall downward trend and local recovery, which can be divided into linear information reflecting the global downward trend and nonlinear information reflecting the local recovery phenomenon. In general, the aging of the PEMFC system is the outcome of the aging of individual components. Therefore, it is beneficial to account for differences in the aging time scales of components.

This paper thus proposes a hybrid framework data-driven method to cope with the aging timescale differences in components and voltage recovery phenomenon in PEMFCs. Inspired by recent works for wind speed [30] and battery capacity [31] prediction using signal decomposition methods, the PEMFC aging data in this work are first divided into multiple sequences to reflect the different aging time scales of components. Next, each decomposed sequence is further divided into linear and nonlinear parts, reflecting the overall downward trend and local recovery phenomena within each aging time scale. Then, the two forms of sequences are predicted by a linear time-series method and a nonlinear machine learning approach to improve the prediction effect. Moreover, the attention mechanism is introduced in the machine learning method to improve the prediction accuracy of the nonlinear information. Finally, the predictions for each aging timescale are summed to obtain an overall prediction result. The main novelty of the proposed framework is summarized as follows:

1) The proposed hybrid framework data-driven method has high adaptability to the data. After the PEMFC data is decomposed into different time scales, the data of each time scale is further separated into linear and nonlinear information, and the corresponding methods are used to predict these two parts for better predictive performance.
2) The complete ensemble empirical mode decomposition with adaptive noise (CEEMDAN) method is used to decompose the aging trends of multiple time scales in the raw fuel cell aging data. CEEMDAN is convenient for independent prediction and analysis of each aging time scale.
3) Using the GRU method with an attention mechanism as a prediction method for nonlinear trends further improves the prediction effect.

The paper is organized as follows. First, Section 2 introduces the methodology of the hybrid framework for the data-driven method. Then, Section 3 presents the data processing. Next, in Section 4, the prediction results of the proposed method are analyzed and compared with the results of peer research. Finally, the corresponding conclusions are given in Section 5.

2. Methodology

2.1. Prediction framework

In this work, the output voltage data are used to show the performance of the PEMFC system. Fig. 1 illustrates the framework of the proposed method.

In the proposed framework, the PEMFC voltage data are first decomposed into n intrinsic mode function (IMF) sequences by the CEEMDAN. The nth IMF sequence is also called the residual sequence. A fixed-step moving average (MA) method is used for each decomposed sequence to separate the data with linear and nonlinear information. For the linear data, the autoregressive integrated moving average (ARIMA) is used for prediction. Meanwhile, the GRU with the attention mechanism is used for nonlinear information extraction. Next, the linear and nonlinear prediction results are combined to obtain each IMF sequence's prediction. Finally, adding up the prediction results of all IMF sequences yields the final prediction.

2.2. CEEMDAN

The CEEMDAN is significantly improved from the original empirical mode decomposition (EMD) by overcoming the mode-mixing problem [32]. We use the CEEMDAN to decompose the raw PEMFC voltage data $y(t)$ into sequences with different aging time scales. The steps are as follows:

Step 1: Add j ($j = 1, 2, \ldots, k$) Gaussian white noise to the raw voltage data, and a series of new sequences obtained can be expressed as:

$$yj(t) = y(t) + \varepsilon 0 vj(t) \tag{1}$$

where $y_j(t)$ represents the new sequence; ε_0 is a coefficient that

determines the signal-noise ratio; and $v_j(t)$ is the Gaussian white noise.

Step 2: Obtaining a CEEMDAN decomposition sequence for raw voltage data:

$$IMF1 = \frac{\sum_{j=1}^{k} IMFj1}{k} \tag{2}$$

where IMF_1 is the first IMF sequence of $y(t)$ decomposed by CEEMDAN, and IMF_{j1} is the first IMF sequence of the $y_j(t)$ decomposed by EMD. The residual sequence $r_1(t)$ of the $y(t)$ decomposed by CEEMDAN is expressed as:

$$r1(t) = y(t) - IMF1 \tag{3}$$

Step 3: Replace $y(t)$ in Step 1 with $r_1(t)$, and repeat the above steps one and two to get the first IMF sequence of $r_1(t)$ decomposed by CEEMDAN, which is the second IMF sequence of $y(t)$ decomposed by CEEMDAN.

Step 4: Repeat Steps 1 to 3 to obtain multiple IMF sequences of the raw voltage data $y(t)$ until the final residual sequence $r_{n\text{-}1}(t)$ is a monotone function and cannot be decomposed. Then the raw voltage data $y(t)$ can be expressed as:

$$y(t) = \sum_{i=1}^{n-1} IMFi + rn - 1(t) \tag{4}$$

where the nth IMF sequence equals the residual sequence $r_{n\text{-}1}(t)$.

2.3. Prediction method

2.3.1. Moving average

The n decomposed IMF sequences obtained from CEEMDAN represent the aging trends on different time scales. These sequences contain linear and nonlinear information that can be used to predict the aging behavior [28,29,33], and we use moving average (MA) to decompose the sequences to improve the prediction accuracy, i.e.,

$$lt = \frac{1}{m} \sum_{i=t-m+1}^{t} yi \tag{5}$$

$$rt = yt - lt \tag{6}$$

where m is the step size. l_t contains linear information with a stable downward trend, and is suitable for forecasting using linear methods. r_t is the nonlinear component that represents the local fluctuation information, and it should be used for nonlinear forecasting methods.

2.3.2. Autoregressive integrated moving average

Based on the linear component, an ARIMA model is trained for each IMF sequence. The ARIMA treats the value y_t at the current moment as a linear function f of past observations, i.e.,

$$yt = f(yt-1, yt-2, \cdots, yt-p, \varepsilon t-1, \varepsilon t-2, \cdots, \varepsilon t-q) \tag{7}$$

where $y_{t\text{-}1}$, $y_{t\text{-}2}$, …, $y_{t\text{-}p}$ are the past voltage measurements and $\varepsilon_{t\text{-}1}$, $\varepsilon_{t\text{-}2}$, …, $\varepsilon_{t\text{-}q}$ are measurement errors with zero mean and constant variance. In particular, p and q are the autoregressive order and the moving average order, respectively, and their values are determined during model training. As a linear method, it is necessary to ensure that the data input into ARIMA is stable. Otherwise, a pre-difference process is essential. The parameter d is the order of the difference process. When the differential process is not required, d is taken as 0. In summary, p, d, and q are the three most important parameters of ARIMA.

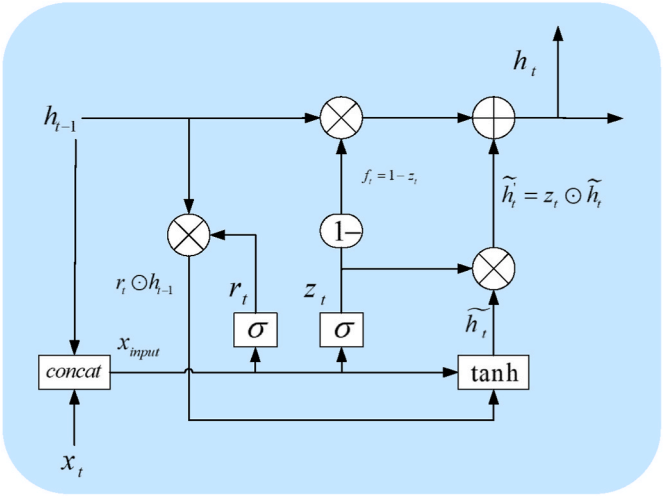

Fig. 2. GRU structure diagram.

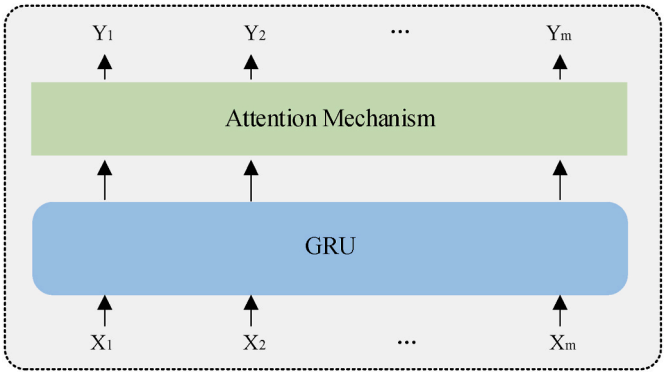

Fig. 3. Schematic diagram of GRU with the attention mechanism.

2.3.3. GRU with attention mechanism

Compared to widely used LSTM, GRU has many advantages in improving the effect of long sequence prediction and it is therefore adopted for nonlinear sequence prediction [34]. The structure of the traditional GRU is shown in Fig. 2 and is governed by.

$$zt = \sigma(Wz \cdot [ht-1, xt]) \tag{8}$$

$$rt = \sigma(Wr \cdot [ht-1, xt]) \tag{9}$$

$$\tilde{ht} = \tanh(WH[rt \odot ht-1, xt]) \tag{10}$$

$$ht = (1 - zt) \odot ht-1 + zt \odot \tilde{ht} \tag{11}$$

where W_z, W_r, and W_h are the network weights of the update gate, the reset gate, and the candidate states, respectively.

In Eq. (10), the reset gate combines the previous neuron's hidden state $h_{t\text{-}1}$ with the current neuron's input x_t to obtain a candidate hidden state $\sim h_t$. $\sim h_t$ mainly contains the input of the current neuron, so the function of the reset gate can be understood as remembering the current neuron's input. In Eq. (11), the update gate controls the ratio of the previous neuron's hidden state $h_{t\text{-}1}$ to the current neuron's hidden state h_t. It can be seen from Eq. (11) that GRU can use the same gate to forget and select (whereas LSTM needs to use multiple gates), thus achieving an optimal structure.

The attention mechanism is introduced into the GRU to improve the prediction performance of the nonlinear information in the IMF sequences. The attention mechanism can generally be used before or after the GRU method. However, using it before the GRU method would cause

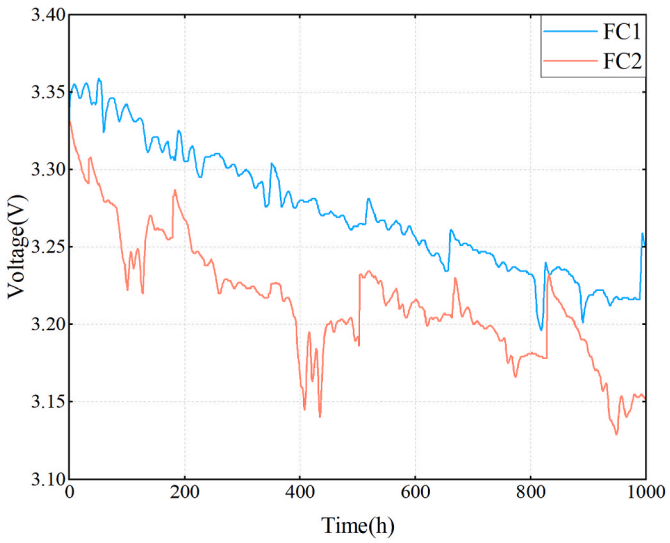

Fig. 4. Relationship between voltages and time of FC1 and FC2.

part of the attention to be distracted by other features, resulting in a decline in the effect of the method [35]. Thus, this paper uses the attention mechanism after the GRU method. First, the input voltage data is converted to multiple feature vectors for GRU training. Then, the feature vectors are used for GRU model training to get the initial output vectors. In order to obtain a reasonable attention distribution, the initial output vectors are used as the input vectors of the attention mechanism, and the corresponding attention weight parameters are calculated. Finally, the final prediction result is obtained. The structure of GRU with the attention mechanism is shown in Fig. 3.

The numbers of input, hidden, and output layers of the GRU are selected as 1, 2, and 1, respectively. The input layer has 60 neurons, each with 100 wt and 100 biases. The first hidden layer has 100 neurons, and each neuron has 80 wt and 80 biases. The second hidden layer has 80 neurons, each with 10 wt and 10 biases. Finally, the output layer has 10 neurons, each containing 1 wt parameter and 1 bias parameter. Introducing the attention mechanism to the GRU increases the attention calculation without affecting the parameter settings of other links in the GRU.

3. Data preprocessing

3.1. Data description

The data used in this work were obtained from the IEEE PHM 2014 Data Challenge, which has been widely used as a benchmark dataset for fuel cell voltage decay prediction. The dataset contains the aging test data of two PEMFC stacks, denoted by FC1 and FC2. The FC1 aging test simulates static working conditions, running for 1154h at a steady current of 70 A. The FC2 aging test simulates quasi-dynamic working conditions, running 1020h at 70 A dynamic current and 7 A oscillating current. The overall voltage changing trends for two fuel cells over the first 1000h with 1h intervals are shown in Fig. 4.

To measure the physical state of the fuel cell's internal components, the fuel cell is periodically shut down [20]. During these periods, some components inside the fuel cell recovered, resulting in a voltage recovery [21–24]. The phenomenon of voltage recovery complicates the aging mechanism of fuel cells and makes the prediction more difficult. Nevertheless, based on the decomposition idea and the hybrid framework, the proposed method predicts this voltage recovery better.

3.2. CEEMDAN decomposition

The decomposition results of FC1 and FC2 based on CEEMDAN are

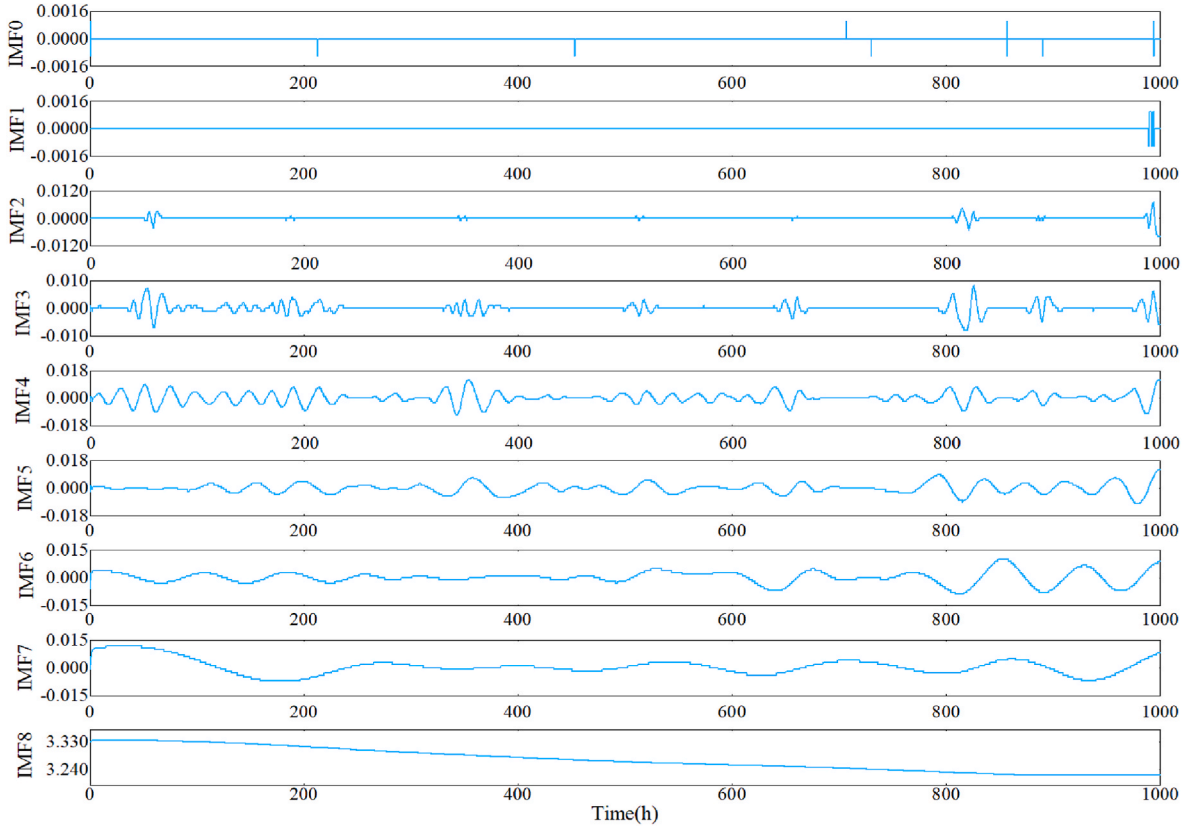

Fig. 5. CEEMDAN decomposition results of FC1.

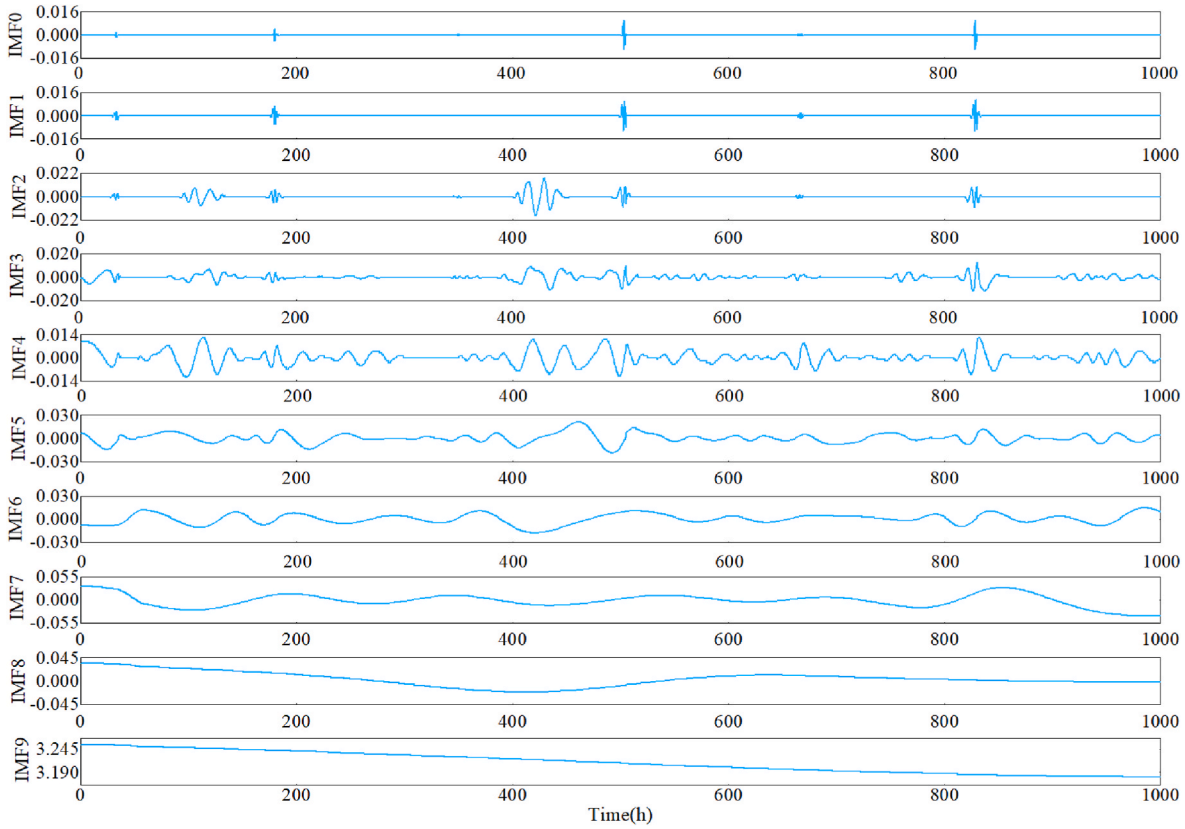

Fig. 6. CEEMDAN decomposition results of FC2.

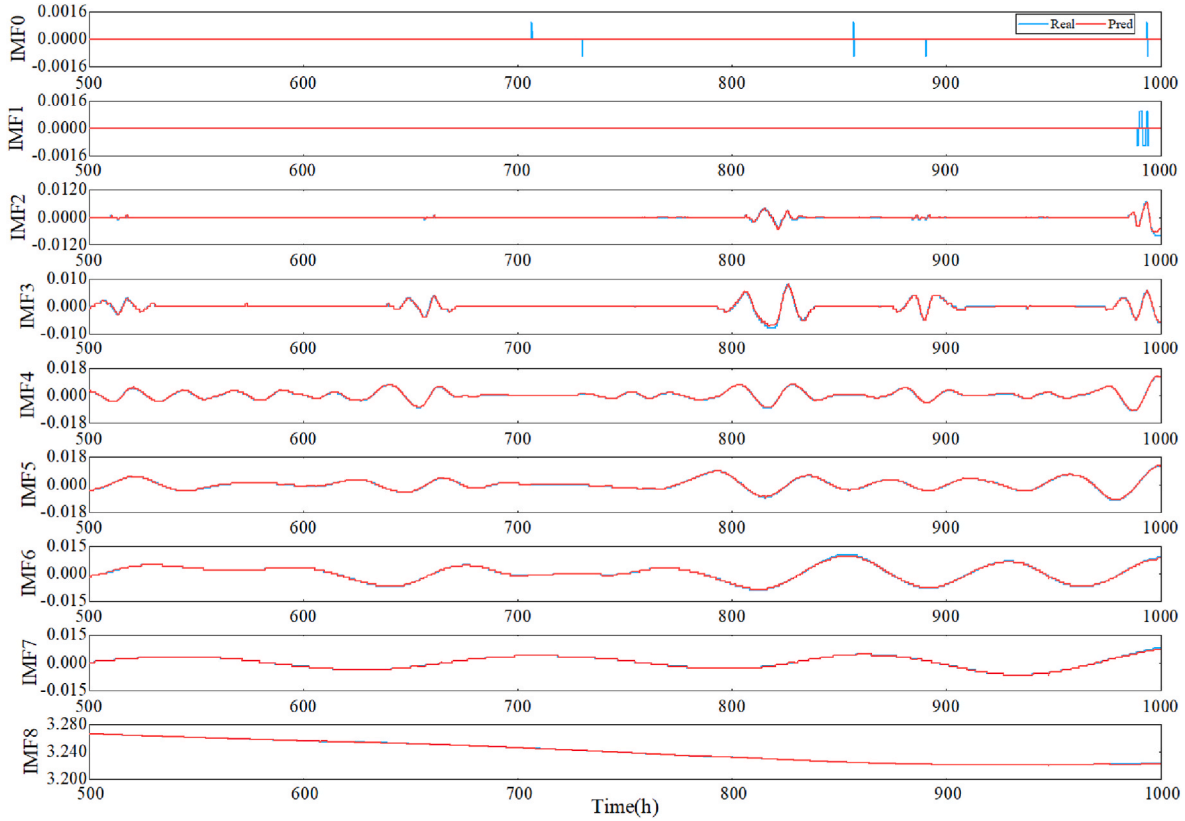

Fig. 7. FC1 sequence prediction results.

Table 1
FC1 sequence prediction errors($\times 10^{-3}$).

IMF	0	1	2	3	4	5	6	7	8
MAE	0.009	0.010	0.064	0.141	0.305	0.154	0.196	0.112	0.098
RMSE	0.054	0.093	0.064	0.295	0.385	0.277	0.311	0.211	0.184

shown in Figs. 5 and 6. The nine IMF sequences of the FC1 represent the aging conditions of different aging time scales with different trends and ranges. The residual (IMF8) drops from 3.33 to 3.24, and it reflects the most dominant aging trend. IMF0-IMF7 are relatively small with nonlinear trends, which may reflect the fuel cell's local change characteristics and recovery phenomena. Specifically, the components IMF2 to IMF7 have a changing trend similar to a periodic function. Although the exact correspondence between the IMF sequences and the internal components of fuel cells is unclear, it can still be considered that the changing trends of these IMF sequences include the overall aging trends and local recoverable phenomena of the components. On the other hand, the local changes of IMF0-IMF1 are not regular but impulsive. Further investigation is required to determine whether recovery phenomena or unexpected noises cause these trends.

For FC2 data, ten IMF sequences are obtained. Like FC1, the residual (IMF9) is the largest component with a clear downward aging trend among these sequences. On the other hand, IMF0 to IMF8 vary periodically, which may reflect the components' aging trend and recovery phenomenon. Likewise, the significance of impulse-function-like trends in IMF1 must be further determined.

4. Results and discussion

The prediction effects of various methods are evaluated and compared based on three metrics: mean absolute error (MAE), root mean square error (RMSE), and mean absolute percentage error (MAPE), i.e.,

$$MAE = \frac{1}{N}\sum_{i=1}^{N}|yi - \widehat{yi}| \tag{12}$$

$$RMSE = \sqrt{\frac{1}{N}\sum_{i=1}^{N}(yi - \widehat{yi})^2} \tag{13}$$

$$MAPE = \frac{100}{N}\cdot\sum_{i=1}^{N}\left|\frac{yi - \widehat{yi}}{yi}\right| \tag{14}$$

where N is the number of test data, y_i is the real value, and $\hat{y}_i$ is the predicted value.

4.1. FC1 prediction results

This section analyzes the prediction results using the proposed method on FC1 data. Then, comparisons are made with various methods to demonstrate the advantages of the hybrid framework with the attention mechanism.

4.1.1. Analysis of hybrid-attention

In this section, the prediction results of the proposed method on FC1 data are analyzed. In detail, the first 500h of data are used to train the proposed model, and then this model is tested on the last 500h. Raw voltage data are decomposed into sequences of multiple aging timescales. Then, the sequences are further decomposed into linear and nonlinear components, and corresponding predictions are made using ARIMA and GRU methods with attention mechanisms. The prediction results for the sequences are shown below.

Fig. 7 shows the true and predicted IMF0 to IMF8 sequences, and the corresponding errors are given in Table 1. It should be noted that the calculated MAPEs are not included for comparison since they are much smaller than MAEs and RMSEs. The small MAE and RMSE results demonstrate the high precision of this prediction. Especially for IMF0 and IMF1, most of the predicted values closely match the real values. Although the true value locally exhibits positive and negative pulse characteristics according to Eq. (12) and Eq. (13), the excellent prediction effect at other times reduces the adverse effects of this characteristic, making the calculated error metrics of IMF0 and IMF1 lower. Compared with IMF0 and IMF1, although the errors from IMF2 to IMF8 are slightly higher, the changing trends of the real value and the predicted value are the same.

As shown in Fig. 8 and Table 2, there is a good correlation between the predicted and real voltages of the FC1. As a result of the accumulation of forecast trends in each IMF subsequence, the overall forecast curve largely inherits the advantage of high precision, as well as some errors in some subsequences. Specifically, Fig. 8 shows that the predicted value at 820h is slightly higher than the corresponding real value, where this high probability results from the prediction error of the IMF3 subsequence. Likewise, IMF0 and IMF1 are most likely responsible for

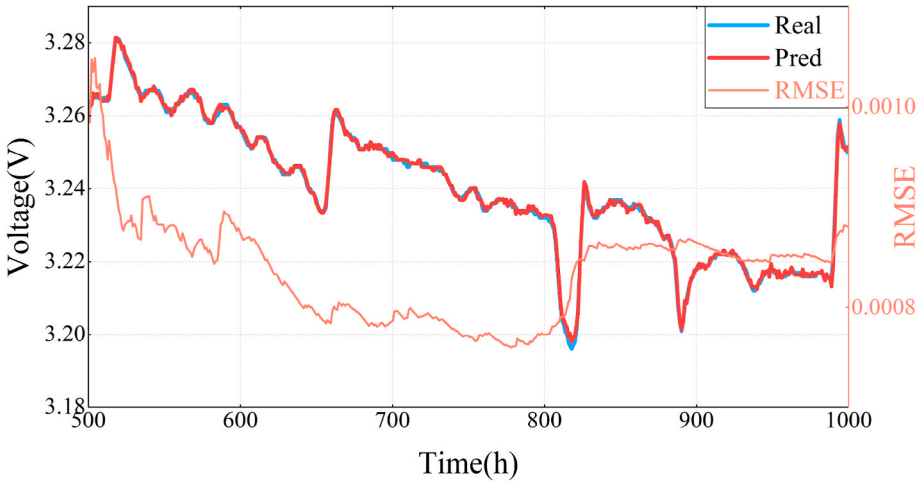

Fig. 8. FC1 final prediction results.

Table 2
FC1 multi-training length prediction errors.

Train (h)	Metric	ARIMA	LSTM	GRU	Hybrid-LSTM	Hybrid-GRU	Hybrid-Attention
500	MAE	0.001315	0.001492	0.001085	0.000920	0.000863	**0.000688**
	RMSE	0.002589	0.002047	0.001548	0.001247	0.001178	**0.000882**
	MAPE	0.040604	0.046141	0.033562	0.028436	0.026631	**0.021125**
600	MAE	0.001391	0.001166	0.001113	0.000852	0.000844	**0.000666**
	RMSE	0.002777	0.001981	0.001639	0.001154	0.001159	**0.000939**
	MAPE	0.043026	0.036094	0.034450	0.026344	0.026115	**0.020590**
700	MAE	0.001415	0.001407	0.001343	0.001080	0.000862	**0.000631**
	RMSE	0.002952	0.002154	0.001892	0.001452	0.001201	**0.000821**
	MAPE	0.043828	0.043564	0.041592	0.033458	0.026713	**0.019541**
800	MAE	0.001785	0.001568	0.001186	0.001169	0.001029	**0.000692**
	RMSE	0.003562	0.002278	0.002360	0.001597	0.001450	**0.000957**
	MAPE	0.055318	0.048631	0.036793	0.036262	0.031914	**0.021474**

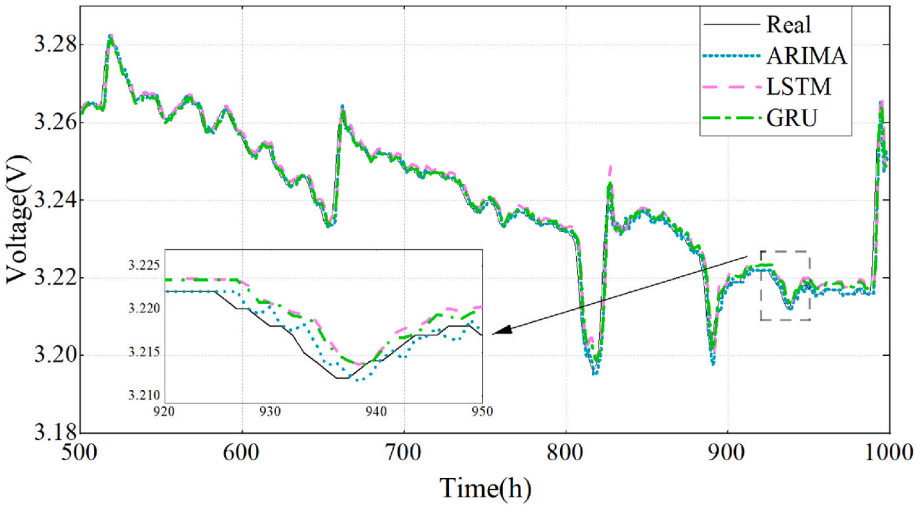

Fig. 9. Individual predictions for multiple methods of FC1.

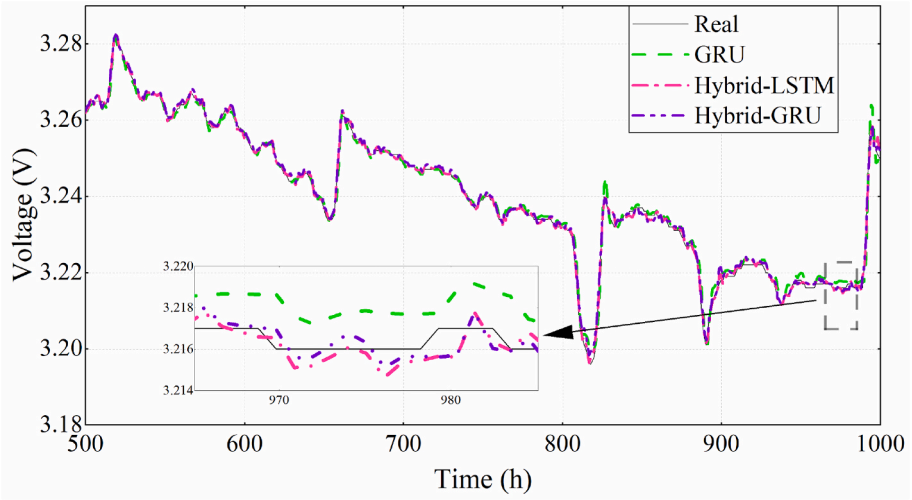

Fig. 10. Predictions for hybrid methods of FC1.

the slight error of the overall forecast curve at the peak at 990h.

The RMSE error curve depicted in Fig. 8 provides a visual representation of the trend of cumulative prediction error with aging time. Notably, during the interval from 510h to 820h, a discernible downward trend is observed in the RMSE values. This drop means that under the root sign on the right-hand side of Eq. (13), the denominator grows faster than the numerator. The denominator N increases linearly with the aging time. Therefore, it can be deduced that the sum of squared errors represented by the numerator grows slowly, which indicates that the proposed method exhibits stable prediction errors.

It is worth highlighting that the sharp voltage fluctuations at 660h, 820h and 990h all have a considerable impact on RMSE. It is obvious

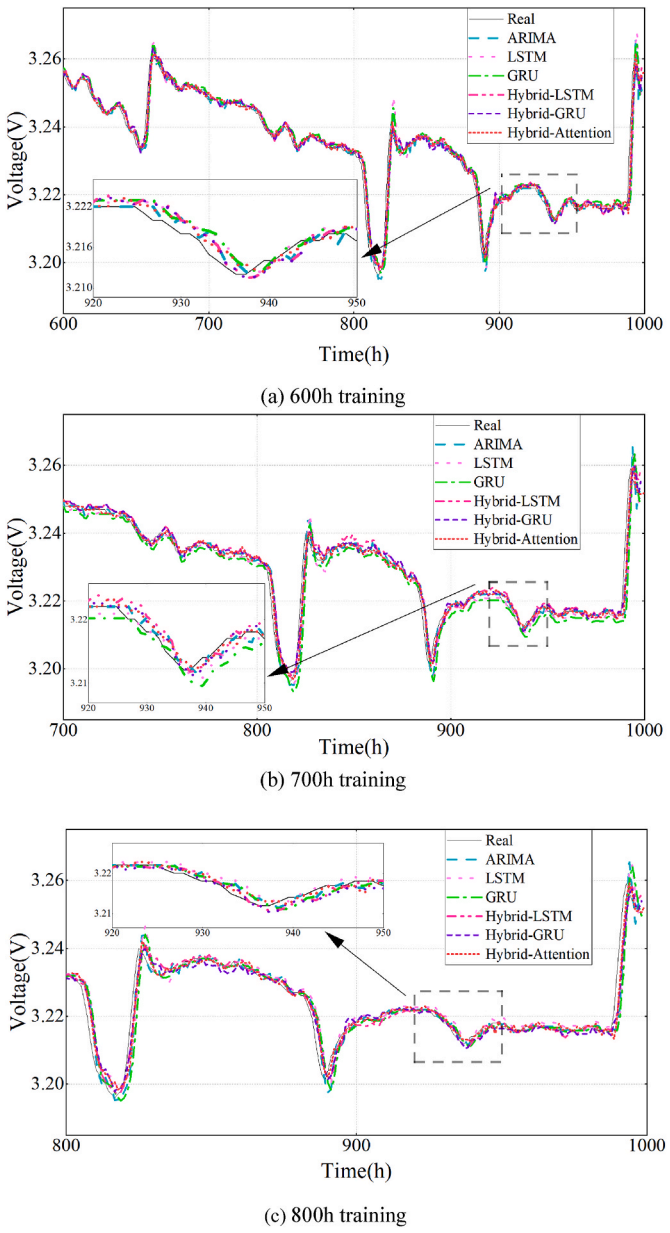

(a) 600h training

(b) 700h training

(c) 800h training

Fig. 11. FC1 multi-training length prediction.

that the RMSE increase at 820h is the largest, which indicates that when the voltage fluctuation is too large, the prediction error of the proposed method increases significantly, leading to a degradation in prediction performance.

4.1.2. Comparative study of multiple methods

This section illustrates the advantages of the proposed hybrid framework from two aspects. The first 500h of data are used for training of the proposed model to demonstrate the superiority of the hybrid framework. Then, the data of the first 600h, 700h, and 800h are used for training to prove the applicability of the proposed method further.

4.1.2.1. Analysis of hybrid framework. To demonstrate the superiority of the proposed framework, it is necessary to discuss the performance of each method separately. Fig. 9 presents the prediction effect of each method independently. The best prediction performance of the methods is used for the comparative analysis of hybrid framework predictions in Fig. 10.

There are always over-predictions in individual predictions. Around the troughs at 820h and 890h, the ARIMA predictions are too low. Around the peaks around 660h, 840h, and 990h, the predictions of LSTM and GRU are too high, and the result of LSTM is the highest. Outside these peaks and troughs, ARIMA's predicted values are closer to the real values, and this phenomenon is most evident in the prediction from 920 to 950h. However, it can be seen from the enlarged picture that the prediction results of LSTM and GRU are steadier, while the prediction results of ARIMA always have severe fluctuations.

As a linear method, ARIMA's predictions are closer to the real value but vary more widely. The disadvantages of ARIMA outweigh its advantages, so its results are not optimal. GRU has a simpler structure and performs better among the neural network methods, so it is used as a representative of the individual methods for the following comparisons.

Fig. 10 shows prediction results using a hybrid prediction framework to demonstrate its superiority. The hybrid prediction framework consists of two parts: a linear part based on ARIMA, a nonlinear part based on LSTM or GRU, and finally, the linear and nonlinear components are combined. The hybrid framework alleviates the overprediction of the peaks and troughs of the individual method. Most evidently, this improvement can be seen from the peak predictions for 840h and 990h. In the peak prediction at 660h and the trough prediction at 820h and 890h, the results of the individual method and the hybrid methods are close. Likewise, the prediction for 965h–985h is zoomed in for further discussion. The predicted value of the hybrid method is closer to the real value, which shows that the prediction performance of the hybrid method is significantly better than that of the individual method. Neural networks are used to predict the regularity recovery trend of nonlinear nature. ARIMA is used to predict the linear part, which captures the overall stable downward trend and improves the prediction effect. The prediction effect of the Hybrid-GRU method is better than that of the Hybrid-LSTM method. Thus, the composition algorithm can further improve the accuracy of the hybrid framework.

4.1.2.2. Comparative analysis. Based on the hybrid framework, an attention mechanism is introduced into GRU to further improve the prediction effect. The first 600h, 700h, and 800h of FC1 data are used to train the proposed method and related method. Their prediction results are shown in Fig. 11. To intuitively display the performance of each method under different training data lengths, the errors are shown in Table 2 and Fig. 12 respectively.

As shown in Table 2, the prediction error of ARIMA is the largest under the training length of 600h, 700h and 800h. As FC1 data vary nonlinearly, neural networks outperform ARIMA. Moreover, as the training length increases, the prediction error of ARIMA keeps increasing. When the training length is short, the longer test data makes the fluctuation of ARIMA prediction results less obvious. Therefore, increasing the training length has the adverse effect of this drastic change more apparent, leading to an increase in prediction error, which is not seen in the LSTM and GRU prediction results. In the proposed hybrid framework, the nonlinear part in the sequence is predicted using the neural network-based methods. This improves the prediction accuracy.

The error comparison shows the superiority of the proposed method in this work. With the proposed hybrid framework and attention mechanism, the proposed method shows the best prediction performance. Compared to the traditional GRU, the prediction effect of the Hybrid-LSTM method has increased by 1.4%–23.5%, and the effect of the Hybrid-GRU method has increased by 13.2%–35.8%. Furthermore, the prediction performance of the proposed Hybrid-Attention method is 20.3%–32.8% better than that of the Hybrid-GRU method and 36.6%–53.0% better than that of the individual GRU method.

4.2. FC2 prediction results

Similarly, this section analyzes and shows the prediction effect of the proposed method using the FC2 data. Then, the comparison

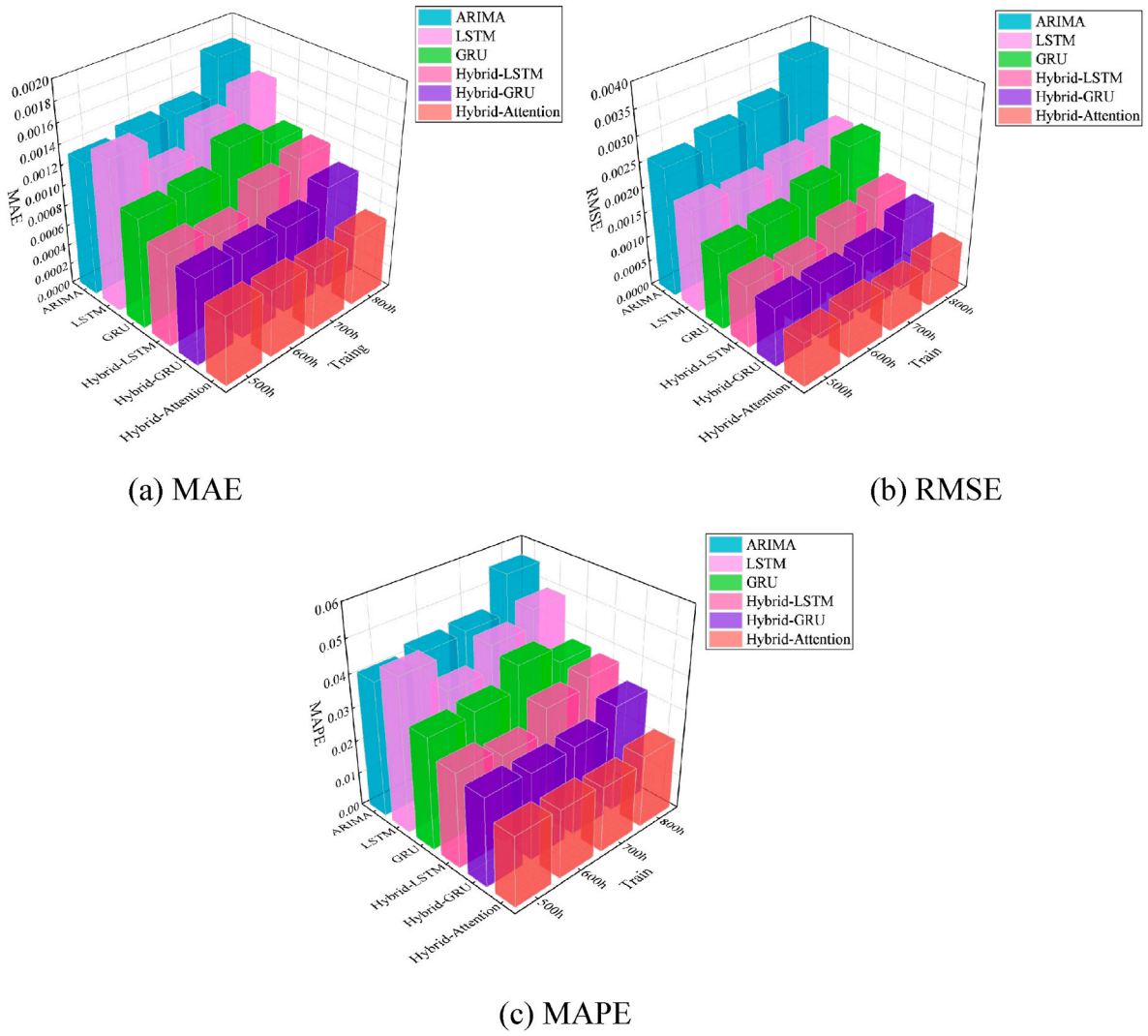

Fig. 12. FC1 multi-training length prediction errors.

demonstrates the advantages of the proposed hybrid framework and attention mechanism.

4.2.1. Analysis of hybrid-attention

In this section, the prediction results of the proposed method on the FC2 data are analyzed. The first 500h of data is used to train the proposed model, and then this model is tested on the last 500h of data. The raw voltage data are decomposed into sequences of multiple aging time scales and are further decomposed into linear and nonlinear parts for separate predictions. The prediction results for the sequence are shown below.

The prediction results of IMF0 to IMF9 sequences are shown in Fig. 13 and Table 3. Similar to FC1, changes in characteristics like positive and negative pulses cannot be accurately predicted in IMF0 and IMF1, and the prediction effect cannot neutralize their influence on the calculation of the metrics at other times. Compared with IMF0 and IMF1, the true and predicted values from IMF2 to IMF9 have the same change trend.

According to Fig. 14, there is a good correlation between the predicted and real values of the FC2 voltage. The overall forecast trend shows a high degree of confidence. Comparing the RMSE curve in Fig. 14 with that in Fig. 8, it can be found that the prediction error of FC2 remains stable, although it is larger than that of FC1. And the same as in FC1, the sharp voltage fluctuation at 660h and 840h also caused the increase of RMSE, resulting in the decline of prediction performance. Overall, the proposed method exhibits stable predictive performance for the quasi-dynamic working conditions FC2, thus showing the advantage of the proposed hybrid attention method.

4.2.2. Comparative study of multiple methods

This section further illustrates the prediction performance of the proposed hybrid framework on the FC2 data. The applicability of the proposed method is demonstrated through experiments using the training data of four lengths.

4.2.2.1. Analysis of hybrid framework. As shown in Fig. 15, individual methods still have the disadvantage of over-prediction. Around the troughs at 950h and 970h, The ARIMA predictions are too low. Around the peaks around 510h and 840h, LSTM and GRU make too high predictions. However, unlike the situation in FC1, the data for FC2 changes more drastically. So, the overprediction of ARIMA is not as significant as in FC1. As GRU has the best performance among the individual methods, it is used as the comparison object in the hybrid framework method.

Fig. 16 shows the prediction effect of the hybrid framework on the FC2 data. The hybrid framework improves peak and trough prediction by combining the linear and nonlinear methods. Around the troughs at 950h and 970h, the hybrid framework made accurate predictions. Around the peaks at 510h and 840h, the overprediction of the hybrid

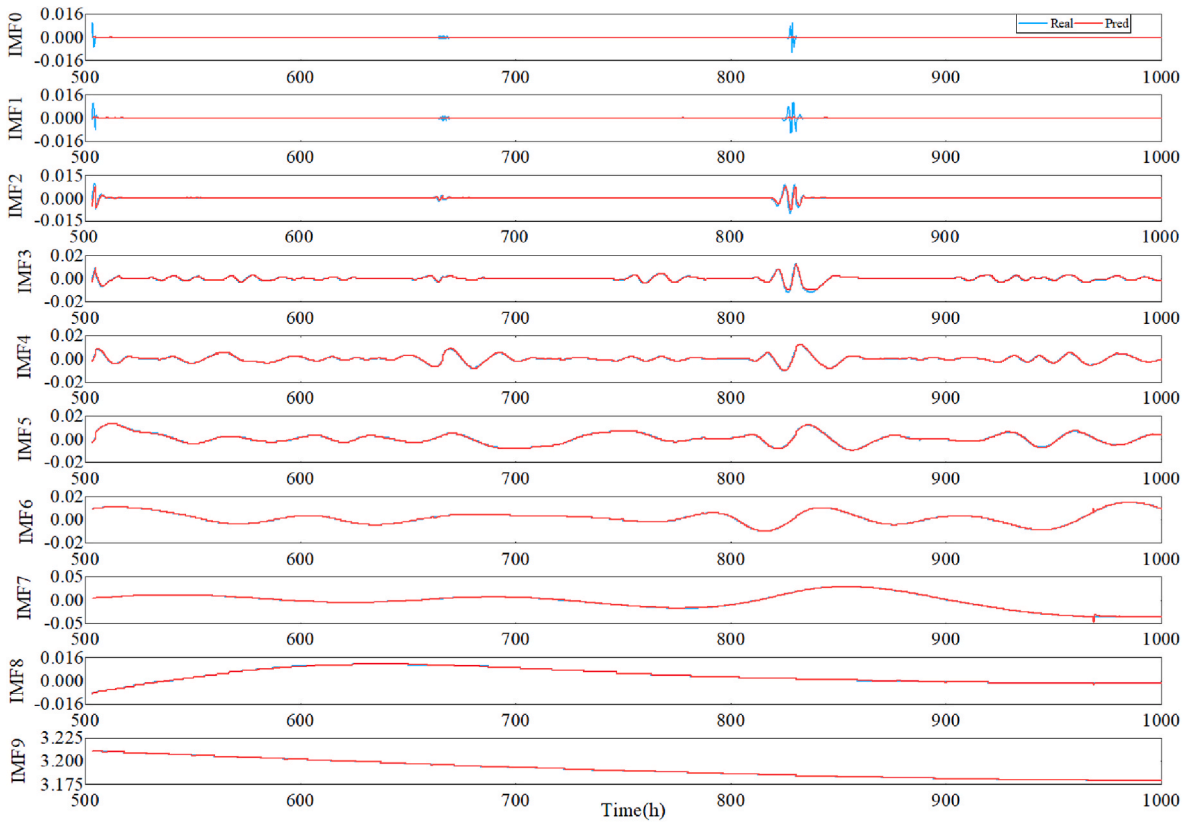

Fig. 13. FC2 sequence prediction results.

Table 3
FC2 sequence prediction errors ($\times 10^{-3}$).

IMF	0	1	2	3	4	5	6	7	8	9
MAE	0.146	0.159	0.281	0.217	0.221	0.214	0.138	0.243	0.035	0.043
RMSE	0.546	0.859	0.554	0.485	0.382	0.320	0.265	0.593	0.123	0.195

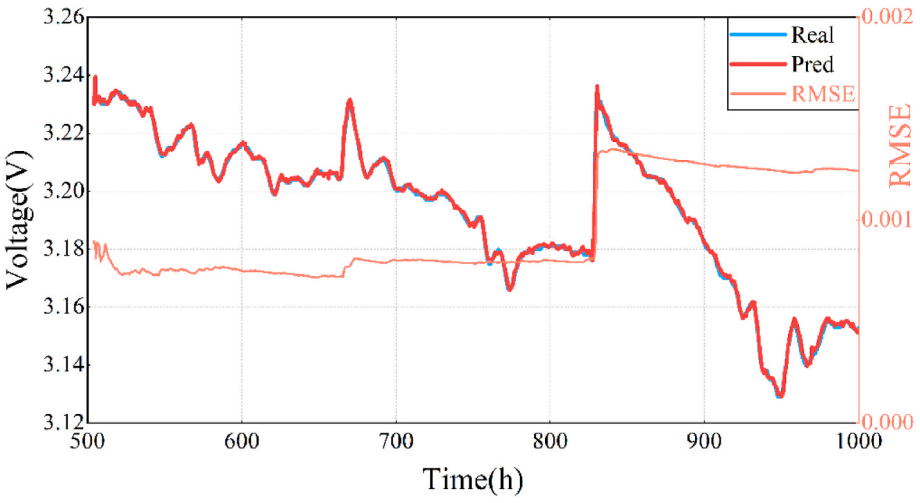

Fig. 14. FC2 final prediction results.

framework is smaller than that of the individual method. Furthermore, the hybrid framework improves local prediction accuracy, which is more evident using the FC2 data.

4.2.2.2. Comparative analysis. To further improve the prediction accuracy, the attention mechanism is further introduced into the hybrid framework, and the prediction results are shown in Fig. 17. To more intuitively display the performance of each method under different training data lengths, the training error metrics are shown in Table 4 and Fig. 18.

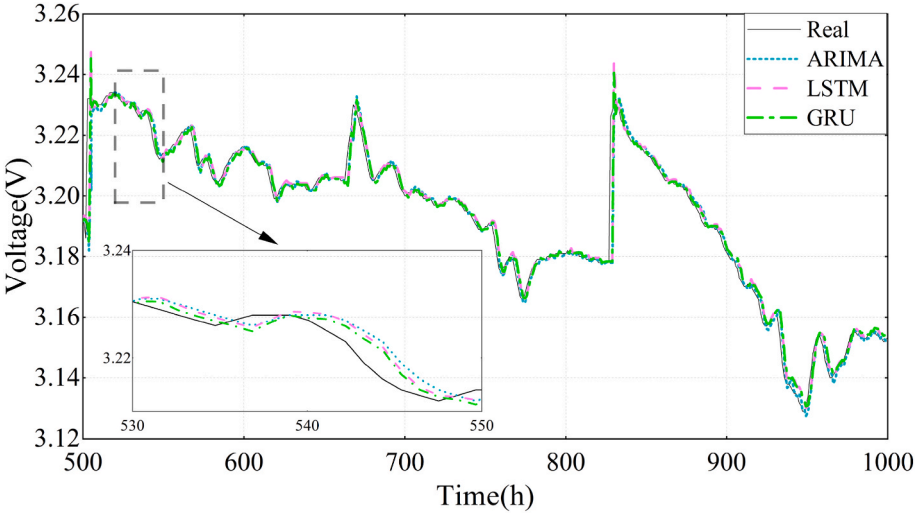

Fig. 15. Individual predictions for multiple methods of FC2.

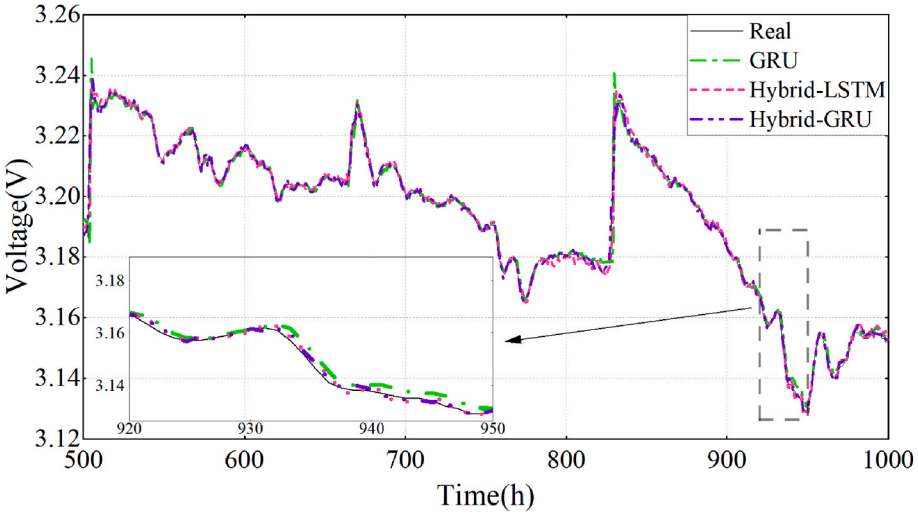

Fig. 16. Predictions for hybrid methods of FC2.

As shown in Table 4, ARIMA has the largest prediction error, which is also the case for FC1. Furthermore, as the length of the training length increases, the prediction error of ARIMA first decreases and then increases. As the data of FC2 varied more drastically than those of FC1, changes in training length have less impact on ARIMA prediction error, and this phenomenon is different from those of FC1. Using FC2, LSTM and GRU prediction errors are not significantly affected by the training length, which is the same phenomenon as in FC1.

The superiority of the proposed method is significantly demonstrated by the prediction errors in Table 4. Compared to the GRU, the prediction performance of the hybrid-LSTM is improved by 2.3%–16.4%, and the prediction effect of the hybrid-GRU method is improved by 6.1%–21.6%. Furthermore, compared to the hybrid-GRU, the hybrid-attention method outperforms the other three training lengths, achieving an improvement of 35.7%–46.0%.

4.3. Comparison of the proposed method with the existing methods in the literature

The prediction error of the proposed method in this work is compared with the results of the existing methods, and the comparison results are given in Table 5. It is worth noting that some prediction accuracies are not included in these methods, as indicated by "-".

To improve noise immunity, Xie et al. proposed an singular spectrum analysis and deep gaussian process (SSA-DGP) method in 2020 [36]. Both the SSA-DGP and the proposed method use the data preprocessing procedure. However, the proposed method improves the prediction accuracy by 77.4%–83.7% in terms of MAE and 83.0%–84.2% in RMSE under the 550h and 650h training conditions.

Wang et al. proposed a bi-directional long short-term memory recurrent neural network with an attention mechanism (BiLSTM-AT) model in 2020 [37]. Compared to LSTM and LSTM with the attention mechanism, the accuracy of BiLSTM-AT has been significantly improved. With the hybrid framework, our proposed Hybrid-AT method achieves further prediction improvement. Specifically, according to MAE, the proposed method improves the prediction accuracy by 56.5%–62.5% on FC1 and 61.8%–70.1% on FC2. According to MAPE, the proposed method improves the prediction accuracy by 42.6%–51.0% on FC1 and 35.0%–54.6% on FC2.

In 2019, Liu et al. [38] proposed an Adaptive neuro-fuzzy inference system based on subtractive clustering (ANFIS-SC), which could improve the prediction effect by adjusting the model parameters. This method combines the neural network with the fuzzy reasoning system, and its superiority is validated by comparing it with the Elman neural

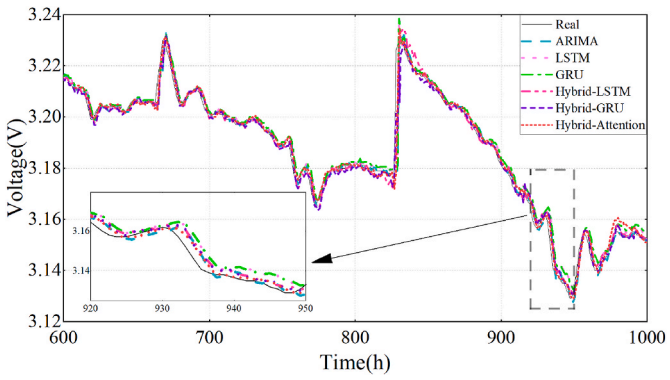

(a) 600h training

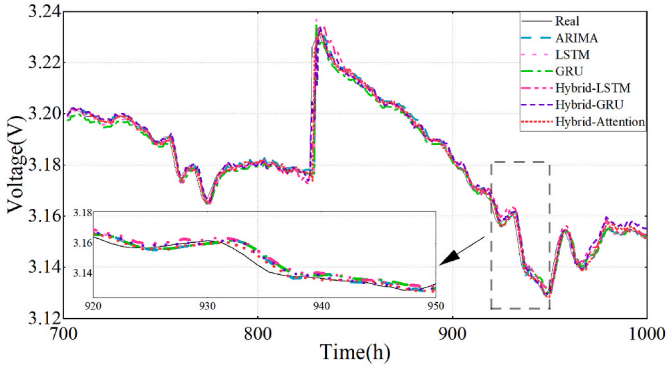

(b) 700h training

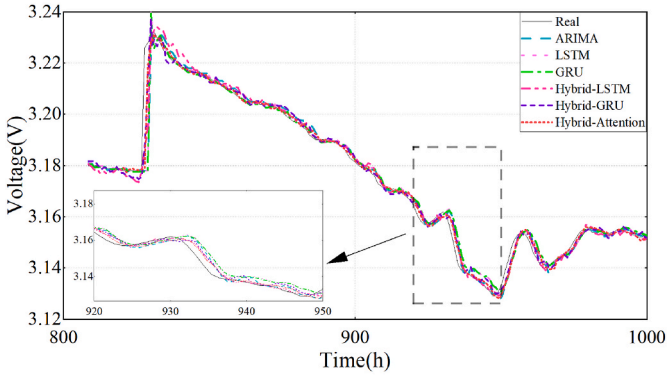

(c) 800h training

Fig. 17. FC2 multi-training length prediction.

network. However, under the condition of 500h training length, the proposed method improves the prediction performance by 73.5% based on RMSE and 74.3% based on MAPE.

To strengthen the prediction results for small data sets, Deng et al. proposed a variational auto-encoded deep gaussian process method in 2022 [39]. Further, under the 600h of training length, the proposed method improves the final prediction performance by 86.9% based on MAE and 90.6% based on RMSE.

The proposed Hybrid-Attention method shows a better prediction performance than the existing mainstream methods. Due to the hybrid framework and the introduced attention mechanism, the proposed method accounts for the difference in aging time scale and the distinction between the linear and nonlinear portions of the prediction model. As a result of these steps, the final prediction performance has been improved.

5. Conclusion

In this paper, a novel hybrid framework is proposed for predicting PEMFC voltage decay by fully exploiting the characteristics of voltage decay data. A large number of performance studies have been carried out to verify the performance of the Hybrid-Attention, and the conclusions are as follows:

1) ARIMA and attention-based GRU are adopted to predict the linear and nonlinear sub-sequences obtained from CEEMDAN. Furthermore, the attention mechanism improves the prediction accuracy on nonlinear subsequences, improving the overall prediction performance.
2) The superiority of the proposed method has been verified on the open-source dataset of PEMFC. For static working conditions FC1, the RMSE of the proposed method ranges from 8.21E-4 to 9.57E-4. For quasi-dynamic working conditions FC2, the RMSE of the proposed method ranges from 1.01E-3 to 2.57E-3.
3) Compared with four state-of-the-art data-driven algorithms, the overall prediction accuracy of the proposed method can be improved by 42.6%–84.2% on FC1 and 35.0%–90.6% on FC2.

The proposed method will be extended for a long-term prediction in the future, and more accurate linear/nonlinear forecasting methods will be applied.

CRediT authorship contribution statement

Changzhi Li: Data curation, Investigation, Software, Writing – original draft. **Wei Lin:** Formal analysis. **Hangyu Wu:** Formal analysis, Validation. **Yang Li:** Methodology, Validation. **Wenchao Zhu:** Conceptualization, Data curation, Investigation, Methodology, Writing – original draft. **Changjun Xie:** Conceptualization, Funding acquisition,

Table 4
FC2 multi-training length prediction error comparison.

Train(h)	Metric	ARIMA	LSTM	GRU	Hybrid-LSTM	Hybrid-GRU	Hybrid-Attention
500	MAE	0.002057	0.001795	0.001525	0.001386	0.001221	**0.000785**
	RMSE	0.005063	0.003883	0.003677	0.002927	0.002402	**0.001265**
	MAPE	0.064279	0.055986	0.047623	0.043449	0.038234	**0.024601**
600	MAE	0.001789	0.001892	0.001650	0.001380	**0.001293**	0.001310
	RMSE	0.004129	0.003238	0.003091	0.003042	**0.002388**	0.002570
	MAPE	0.056074	0.059551	0.051923	0.043244	**0.040564**	0.041300
700	MAE	0.001824	0.001681	0.001511	0.001477	0.001419	**0.000766**
	RMSE	0.004521	0.003357	0.003262	0.002719	0.002656	**0.001308**
	MAPE	0.057319	0.052716	0.047436	0.046446	0.044752	**0.024159**
800	MAE	0.002139	0.001342	0.001364	0.001161	0.001195	**0.000760**
	RMSE	0.005404	0.003802	0.003791	0.001858	0.002718	**0.001014**
	MAPE	0.067219	0.042211	0.042846	0.036508	0.037505	**0.023943**

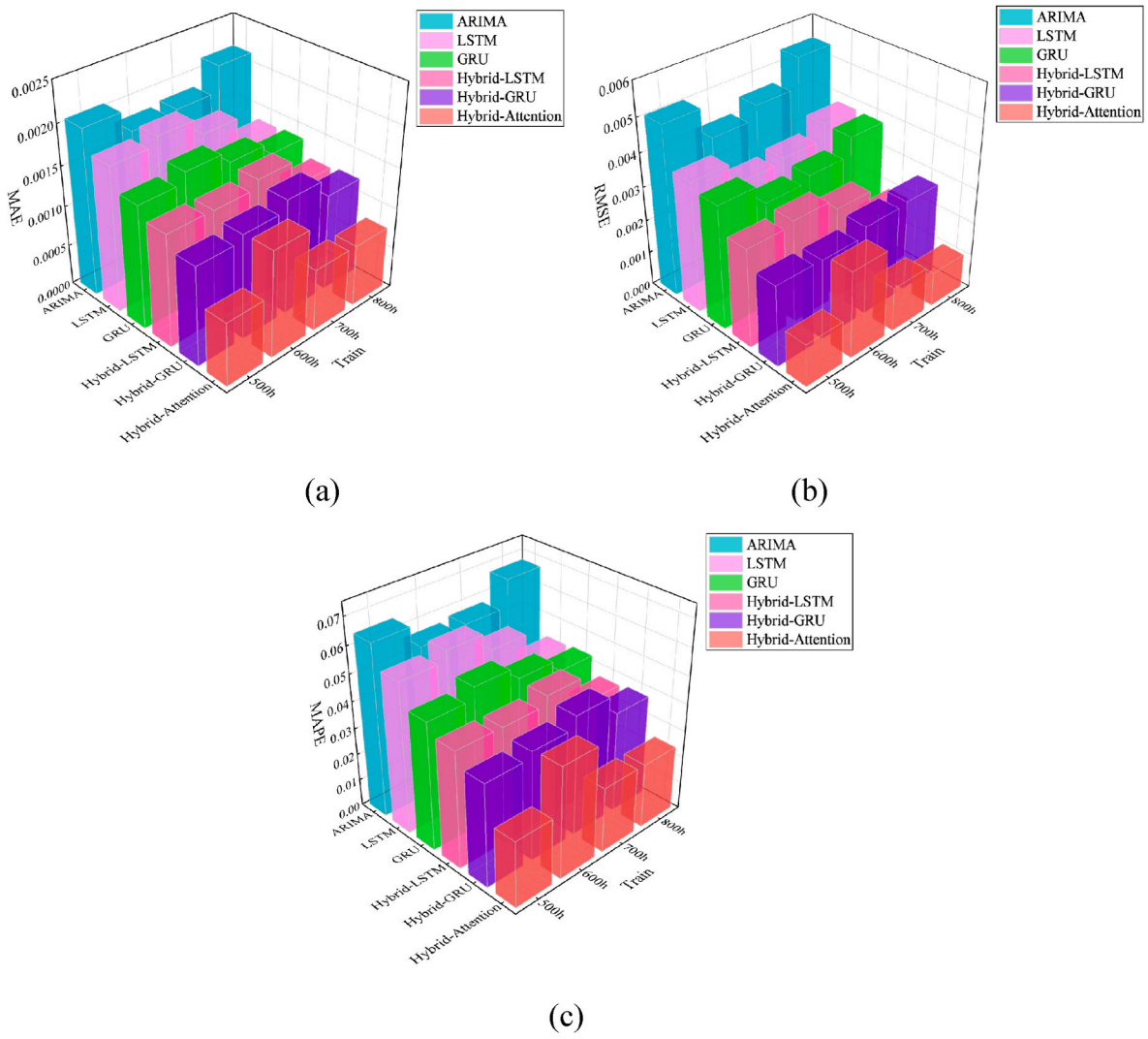

Fig. 18. FC2 multi-training length prediction errors (a) MAE (b) RMSE (c) MAPE.

Table 5
Performance comparison of proposed method with methods in literature.

Data	Train	MAE	RMSE	MAPE	Method
FC1	550	0.0043	0.0057	-	SSA-DGP [36]
	650	0.0031	0.0047	-	SSA-DGP [36]
	600	-	0.0024	0.0420	BiLSTM-AT [37]
	700	-	0.0023	0.0340	BiLSTM-AT [37]
	550	0.0007	0.0009	-	Proposed
	600	-	0.0009	0.0206	Proposed
	650	0.0006	0.0008	-	Proposed
	700	-	0.0010	0.0195	Proposed
FC2	500	-	0.0049	0.0959	ANFIS-SC [38]
	600	-	0.0087	0.0635	BiLSTM-AT [37]
	700	-	0.0034	0.0533	BiLSTM-AT [37]
	600	0.0061	0.0278	-	VAE-DGP [39]
	500	-	0.0013	0.0246	Proposed
	600	0.0008	0.0026	0.0413	Proposed
	700	-	0.0013	0.0242	Proposed

Project administration, Supervision, Writing – review & editing. **Hoay Beng Gooi:** Supervision, Writing – review & editing.

Declaration of competing interest

The authors declare that they have no known competing financial interests or personal relationships that could have appeared to influence the work reported in this paper.

Acknowledgments

This work was supported by the National Key Research and Development Program of China (2020YFB1506802), China Scholarship Council (202106950031) and the Office of Naval Research Global (ONRG), USA under CODE 33D, Naval Energy Resiliency and Sustainability in Broad Agency Announcement N00014-18-S-B001, and ONRG award number: N62909-19-1-2037.

References

[1] Z. Xu, W. Xu, E. Stephens, B. Koeppel, Mechanical reliability and life prediction of coated metallic interconnects within solid oxide fuel cells, Renew. Energy 113 (2017) 1472–1479, https://doi.org/10.1016/j.renene.2017.06.103.
[2] M. Yue, S. Jemei, N. Zerhouni, R. Gouriveau, Proton exchange membrane fuel cell system prognostics and decision making: current status and perspectives, Renew. Energy 179 (2021) 2277–2294, https://doi.org/10.1016/j.renene.2021.08.045.
[3] Y. Zou, Y. Xu, X. Feng, R.T. Naayagi, B. Soong, Transactive energy systems in active distribution networks: a comprehensive review, CSEE Journal of Power and Energy Systems 8 (5) (2022) 1302–1317, https://doi.org/10.17775/CSEEJPES.2021.03290.
[4] Wenchao Zhu, Bingxin Guo, Li Yang, Yang Yang, Changjun Xie, Jiashu Jin, et al., Uncertainty quantification of proton-exchange-membrane fuel cells degradation prediction based on Bayesian-Gated Recurrent Unit, eTransportation 16 (2023), 100230, https://doi.org/10.1016/j.etran.2023.100230.

[5] Z. Hua, Z. Zheng, E. Pahon, M.-C. Péra, F. Gao, A review on lifetime prediction of proton exchange membrane fuel cells system, J. Power Sources 529 (2022), 231256, https://doi.org/10.1016/j.jpowsour.2022.231256.
[6] Dafeng Zhu, Bo Yang, Yuxiang Liu, Zhaojian Wang, Kai Ma, Xinping Guan, Energy management based on multi-agent deep reinforcement learning for a multi-energy industrial park, Appl. Energy 311 (2022), 118636, https://doi.org/10.1016/j.apenergy.2022.118636.
[7] Dafeng Zhu, Bo Yang, Liu Qi, Kai Ma, Shanying Zhu, Chengbin Ma, et al., Energy trading in microgrids for synergies among electricity, hydrogen and heat networks, Appl. Energy 272 (2020), 115225, https://doi.org/10.1016/j.apenergy.2020.115225.
[8] K. Javed, R. Gouriveau, N. Zerhouni, D. Hissel, Improving accuracy of long-term prognostics of PEMFC stack to estimate remaining useful life, in: 2015 IEEE International Conference on Industrial Technology (ICIT), IEEE, Seville, 2015, pp. 1047–1052, https://doi.org/10.1109/ICIT.2015.7125235.
[9] J. Liu, Q. Li, W. Chen, Y. Yan, Y. Qiu, T. Cao, Remaining useful life prediction of PEMFC based on long short-term memory recurrent neural networks, Int. J. Hydrogen Energy 44 (2019) 5470–5480, https://doi.org/10.1016/j.ijhydene.2018.10.042.
[10] B. Long, K. Wu, P. Li, M. Li, A novel remaining useful life prediction method for hydrogen fuel cells based on the gated recurrent unit neural network, Appl. Sci. 12 (2022) 432, https://doi.org/10.3390/app12010432.
[11] Z. Hua, Z. Zheng, M.-C. Pera, F. Gao, Data-driven prognostics for PEMFC systems by different echo state network prediction structures, in: 2020 IEEE Transportation Electrification Conference & Expo (ITEC), IEEE, Chicago, IL, USA, 2020, pp. 495–500, https://doi.org/10.1109/ITEC48692.2020.9161581.
[12] M. Ibrahim, N. Steiner, S. Jemei, D. Hissel, Wavelets-based approach for online fuel cells remaining useful lifetime prediction, IEEE Trans. Ind. Electron. 1–1 (2016), https://doi.org/10.1109/TIE.2016.2547358.
[13] F.-K. Wang, X.-B. Cheng, K.-C. Hsiao, Stacked long short-term memory model for proton exchange membrane fuel cell systems degradation, J. Power Sources 448 (2020), 227591, https://doi.org/10.1016/j.jpowsour.2019.227591.
[14] K. Chen, S. Laghrouche, A. Djerdir, Fuel cell health prognosis using Unscented Kalman Filter: postal fuel cell electric vehicles case study, Int. J. Hydrogen Energy 44 (2019) 1930–1939, https://doi.org/10.1016/j.ijhydene.2018.11.100.
[15] M. Bressel, M. Hilairet, D. Hissel, B. Ould Bouamama, Extended kalman filter for prognostic of proton exchange membrane fuel cell, Appl. Energy 164 (2016) 220–227, https://doi.org/10.1016/j.apenergy.2015.11.071.
[16] D. Zhou, Y. Wu, F. Gao, E. Breaz, A. Ravey, A. Miraoui, Degradation prediction of PEM fuel cell stack based on multiphysical aging model with particle filter approach, IEEE Trans. Ind. Appl. 53 (2017) 4041–4052, https://doi.org/10.1109/TIA.2017.2680406.
[17] M. Moein-Jahromi, M.J. Kermani, S. Movahed, Degradation forecast for PEMFC cathode-catalysts under cyclic loads, J. Power Sources 359 (2017) 611–625, https://doi.org/10.1016/j.jpowsour.2017.05.102.
[18] G.A. Futter, A. Latz, T. Jahnke, Physical modeling of chemical membrane degradation in polymer electrolyte membrane fuel cells: influence of pressure, relative humidity and cell voltage, J. Power Sources 410–411 (2019) 78–90, https://doi.org/10.1016/j.jpowsour.2018.10.085.
[19] H. Liu, J. Chen, D. Hissel, J. Lu, M. Hou, Z. Shao, Prognostics methods and degradation indexes of proton exchange membrane fuel cells: a review, Renew. Sustain. Energy Rev. 123 (2020), 109721, https://doi.org/10.1016/j.rser.2020.109721.
[20] R. Ma, R. Xie, L. Xu, Y. Huangfu, Y. Li, A hybrid prognostic method for PEMFC with aging parameter prediction, IEEE Trans Transp Electrific 7 (2021) 2318–2331, https://doi.org/10.1109/TTE.2021.3075531.
[21] T. Chu, Q. Wang, M. Xie, B. Wang, D. Yang, B. Li, et al., Investigation of the reversible performance degradation mechanism of the PEMFC stack during long-term durability test, Energy 258 (2022), 124747, https://doi.org/10.1016/j.energy.2022.124747.
[22] B. Xiao, J. Zhao, L. Fan, Y. Liu, S.H. Chan, Z. Tu, Effects of moisture dehumidification on the performance and degradation of a proton exchange membrane fuel cell, Energy 245 (2022), 123298, https://doi.org/10.1016/j.energy.2022.123298.
[23] F. Wang, D. Yang, B. Li, H. Zhang, C. Hao, F. Chang, et al., Investigation of the recoverable degradation of PEM fuel cell operated under drive cycle and different humidities, Int. J. Hydrogen Energy 39 (2014) 14441–14447, https://doi.org/10.1016/j.ijhydene.2014.02.023.
[24] B. Decoopman, R. Vincent, S. Rosini, G. Paganelli, P.-X. Thivel, Proton exchange membrane fuel cell reversible performance loss induced by carbon monoxide produced during operation, J. Power Sources 324 (2016) 492–498, https://doi.org/10.1016/j.jpowsour.2016.05.113.
[25] R. Pan, D. Yang, Y. Wang, Z. Chen, Performance degradation prediction of proton exchange membrane fuel cell using a hybrid prognostic approach, Int. J. Hydrogen Energy 45 (2020) 30994–31008, https://doi.org/10.1016/j.ijhydene.2020.08.082.
[26] Y. Li, T. Wik, C. Xie, Y. Huang, B. Xiong, J. Tang, et al., Control-oriented modeling of all-solid-state batteries using physics-based equivalent circuits, IEEE Trans Transp Electrific 8 (2022) 2080–2092, https://doi.org/10.1109/TTE.2021.3131147.
[27] C.N. Babu, B.E. Reddy, A moving-average filter based hybrid ARIMA–ANN model for forecasting time series data, Appl. Soft Comput. 23 (2014) 27–38, https://doi.org/10.1016/j.asoc.2014.05.028.
[28] M. Khashei, M. Bijari, A novel hybridization of artificial neural networks and ARIMA models for time series forecasting, Appl. Soft Comput. 11 (2011) 2664–2675, https://doi.org/10.1016/j.asoc.2010.10.015.
[29] G.P. Zhang, Time series forecasting using a hybrid ARIMA and neural network model, Neurocomputing 50 (2003) 159–175, https://doi.org/10.1016/S0925-2312(01)00702-0.
[30] G. Zhang, D. Liu, Causal convolutional gated recurrent unit network with multiple decomposition methods for short-term wind speed forecasting, Energy Convers. Manag. 226 (2020), 113500, https://doi.org/10.1016/j.enconman.2020.113500.
[31] P. Wang, X. Dan, Y. Yang, A multi-scale fusion prediction method for lithium-ion battery capacity based on ensemble empirical mode decomposition and nonlinear autoregressive neural networks, Int. J. Distributed Sens. Netw. 15 (2019), 155014771983963, https://doi.org/10.1177/1550147719839637.
[32] W. Zhang, Z. Qu, K. Zhang, W. Mao, Y. Ma, X. Fan, A combined model based on CEEMDAN and modified flower pollination algorithm for wind speed forecasting, Energy Convers. Manag. 136 (2017) 439–451, https://doi.org/10.1016/j.enconman.2017.01.022.
[33] C.N. Babu, B.E. Reddy, A moving-average filter based hybrid ARIMA–ANN model for forecasting time series data, Appl. Soft Comput. 23 (2014) 27–38, https://doi.org/10.1016/j.asoc.2014.05.028.
[34] S. Han, Z. Meng, X. Zhang, Y. Yan, Hybrid deep recurrent neural networks for noise reduction of MEMS-IMU with static and dynamic conditions, Micromachines 12 (2021) 214, https://doi.org/10.3390/mi12020214.
[35] W. Shu, F. Zeng, Z. Ling, J. Liu, T. Lu, G. Chen, Resource Demand Prediction of Cloud Workloads Using an Attention-Based GRU Model. 2021 17th International Conference on Mobility, Sensing and Networking (MSN), IEEE, Exeter, United Kingdom, 2021, pp. 428–437, https://doi.org/10.1109/MSN53354.2021.00071.
[36] Y. Xie, J. Zou, C. Peng, Y. Zhu, F. Gao, A novel PEM fuel cell remaining useful life prediction method based on singular spectrum analysis and deep Gaussian processes, Int. J. Hydrogen Energy 45 (2020) 30942–30956, https://doi.org/10.1016/j.ijhydene.2020.08.052.
[37] F.-K. Wang, T. Mamo, X.-B. Cheng, Bi-directional long short-term memory recurrent neural network with attention for stack voltage degradation from proton exchange membrane fuel cells, J. Power Sources 461 (2020), 228170, https://doi.org/10.1016/j.jpowsour.2020.228170.
[38] H. Liu, J. Chen, D. Hissel, H. Su, Short-term prognostics of pem fuel cells: a comparative and improvement study, IEEE Trans. Ind. Electron. 66 (2019) 6077–6086, https://doi.org/10.1109/TIE.2018.2873105.
[39] H. Deng, W. Hu, D. Cao, W. Chen, Q. Huang, Z. Chen, et al., Degradation trajectories prognosis for PEM fuel cell systems based on Gaussian process regression, Energy 244 (2022), 122569, https://doi.org/10.1016/j.energy.2021.122569.